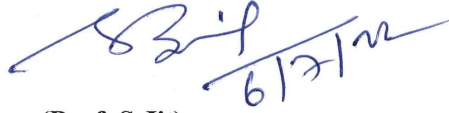


CERTIFICATE

It is certified that the work contained in the thesis titled “**Performance Investigation of Some Heterojunction TFETs on SELBOX Substrates: Application to Dielectric Modulated Label-Free Biosensors**” by “**Ashish Kumar Singh**” has been carried out under my supervision and that this work has not been submitted elsewhere for a degree.

It is further certified that the student has fulfilled all the requirements of Comprehensive Examination, Candidacy and SOTA for the award of Ph. D. Degree.



(Prof. S Jit)

Supervisor

Department of Electronics Engineering

IIT (BHU), Varanasi

प्राचार्य/Professor
इलेक्ट्रॉनिकी अभियांत्रिकी विभाग
Department of Electronics Engineering
भारतीय प्रौद्योगिकी संस्थान
Indian Institute of Technology
(बनारस हिन्दू यूनिवर्सिटी)
(Banaras Hindu University)
वाराणसी/Varanasi-221005

DECLARATION BY THE CANDIDATE

I, Ashish Kumar Singh, certify that the work embodied in this Ph. D. thesis is my own bonafide work and carried out by me under the supervision of Prof. S. Jit from "25/07/2017" to "06/07/2022", at the Department of Electronics Engineering, Indian Institute of Technology (Banaras Hindu University), Varanasi. The matter embodied in this Ph. D. thesis has not been submitted for the award of any other degree/diploma.

I declare that I have faithfully acknowledged, given credits to and referred to the research workers wherever their works have been cited in the text and the body of the thesis. I further declare that I have not willfully copied any other's work, paragraphs, text, data, results, *etc.*, reported in journals, books, magazines, reports dissertations, theses, *etc.*, or available at websites and have not included them in this thesis and have not cited as my own work.

Date: 6/7/2022

Place: Varanasi

Ashish Kumar Singh

Signature of the Student

Ashish Kumar Singh

CERTIFICATE BY THE SUPERVISOR

It is certified that the above statement made by the candidate is correct to the best of my knowledge.

83/9
6/7/22

(Prof. S. Jit)

Supervisor

Department of Electronics Engineering

IIT (BHU), Varanasi

प्राचार्य/Professor
इलेक्ट्रॉनिकी अभियांत्रिकी विभाग
Department of Electronics Engineering
भारतीय प्रौद्योगिकी संस्थान
Indian Institute of Technology
(बनारस हिन्दू यूनिवर्सिटी)
(Banaras Hindu University)
वाराणसी/Varanasi-221005

Signature of Head of Department
"SEAL OF THE DEPARTMENT"

विभागाध्यक्ष/Head
इलेक्ट्रॉनिकी अभियांत्रिकी विभाग
Department of Electronics Engineering
भारतीय प्रौद्योगिकी संस्थान
Indian Institute of Technology
(बनारस हिन्दू यूनिवर्सिटी)
(Banaras Hindu University)
वाराणसी/Varanasi-221005

6/7/22

COPYRIGHT TRANSFER CERTIFICATE

Title of the Thesis: *Performance Investigation of Some Heterojunction TFETs on SELBOX Substrates: Application to Dielectric Modulated Label-Free Biosensor*

Name of the Student: Ashish Kumar Singh

Copyright Transfer

The undersigned hereby assigns to the Indian Institute of Technology (Banaras Hindu University), Varanasi all rights under copyright that may exist in and for the above thesis submitted for the award of the Doctor of Philosophy.

Date: 6/7/2022

Place: Varanasi



Signature of the Student

Ashish Kumar Singh

Note: However, the author may reproduce or authorize others to reproduce material extracted verbatim from the thesis or derivative of the thesis for author's personal use provided that the source and the Institute's copyright notice are indicated.

ACKNOWLEDGEMENT

First and foremost, I would like to thank my supervisor Prof. Satyabrata Jit for his able guidance, appreciation and support. The relentless effort he has put behind is truly commendable. His broad knowledge and enthusiasm for work will always be a source of inspiration for me.

A vote of thanks from the bottom of my heart goes to Prof. V. N. Mishra, Head of Electronics Engineering Department, Indian Institute of Technology (Banaras Hindu University), Varanasi for providing me all the necessary tools and lab facilities to conduct my research work. Besides I would like to thank my REPC members Dr. A. Pandey, Dr. P. C. Pandey for valuable assessment of my research work. I would also like to thank all the faculty members, laboratory staff, librarians and office staff for their kind cooperation and encouragement during this journey.

I am indebted to all my school teachers for the strong foundation they have laid for blossoming of my educational career.

I would like to express my special thanks to my seniors Dr. Kunal Singh, Dr. Sanjay Kumar, Dr. Gopal Rawat, Dr. Sweta Chander, Dr. Hemant Kumar, Dr. Ekta Goel, Dr. Chandan Kumar, Dr. Prince Kumar Singh, Dr. Deepak Kumar Jarwal, Dr. Amit Kumar, Dr. Smriti Ratan, and Dr. Ashwini Kumar Mishra for their guidance. I am thankful to Dr. Kamalaksha Baral, a former PhD Student, IIT BHU, Varanasi and Dr. Manas Ranjan Tripathy, a former PhD Student, IIT BHU, Varanasi, who have been with me for analyzing the technical stuffs. A vote of thanks also goes towards my friendly colleagues Mr. Deep Chand Upadhyay, Dr. Rishibrind Kumar Upadhyay, and Dr. Sanjeev Mani Yadav for keeping a rejoiceful environment. I will also like to thank my juniors from CRME Lab, Mr. Joginder Singh Rana, Mrs. Shikha Singh, Mr. Ankit Kumar Verma, Mr. Varun Kumar Singh and Mr. Prashant Kumar for their friendly suggestions. Especially, I would like to thank my colleagues Mr. Abhinav Pratap Singh and Mr. Vijaya Kumar Devarakonda, for providing a healthy environment for the completion of my thesis. My thanks and deep appreciations also go to all staff members of CRME lab, Department of Electronics Engineering for their kind co-operation.

The thesis could not have been completed without my parent's encouragement and moral support. I would like to express my gratitude, in particular, to my wife "Dr. Nisha Singh" who has stood by me through all my travails, my absences, my fits of pique and impatience. She gave me support and help, discussed ideas and prevented several wrong turns. I appreciate her efforts in taking family responsibilities on my behalf during this phase of my life. Without her constant support it would not be possible for me to complete this journey.

At last, I would like to thank Lord Shiva and Maa Saraswati for giving me the strength, knowledge, ability and opportunity to undertake this research study and to complete it satisfactorily. Without their blessings, this achievement would not have been possible.

Date: 6/7/2022

Ashish Kumar Singh

(Ashish Kumar Singh)

Dedicated
To
My Beloved Son
“Suryansh Singh”

Contents

<i>List of Figures</i>	xv-xxiv
<i>List of Tables</i>	xxv-xxvi
<i>List of Abbreviations</i>	xxvii-xxviii
<i>List of Symbols</i>	xxix-xxx
<i>Preface</i>	xxxi-xxxiii

CHAPTER 1

Introduction and Organization of the Thesis

1.1 Introduction.....	1
1.1.1 Scaling and Power Challenges	1
1.1.2 Limitation of MOSFETs	7
1.1.3 The Emergence of Alternative Devices	9
1.1.3.1 Carbon Nanotube FETs.....	10
1.1.3.2 Graphene FETs	11
1.1.3.3 Nanowire FETs	11
1.1.3.4 Negative Gate Capacitance FETs	12
1.1.3.5 Tunnel Field Effect Transistors (TFETs).....	13
1.1.3.5.1 Physics and Operation of TFETs.....	14
1.1.3.5.2 Subthreshold Swing in TFETs.....	17
1.1.4 Evolution of Tunnel Field Effect Transistors (TFETs).....	18
1.1.5 Adopted Technologies.....	21
1.1.5.1 Gate Oxide Engineering.....	21
1.1.5.2 SiO ₂ /High-k Gate Stacked Engineering.....	21
1.1.5.3 Ferroelectric Oxide Engineering.....	23
1.1.5.4 Substrate Engineering	25
1.1.5.5 Low Bandgap Source Material Engineering.....	27
1.1.6 Circuit and Biosensor based Application using TFETs	28
1.1.6.1 Electronics Circuits Design Based on TFETs.....	29

1.1.7	Biosensors Based on FETs.....	30
1.1.7.1	Types of Biosensors.....	31
1.1.7.2	Structure and Working of the TFET as a Biosensor.....	31
1.1.7.3	Dielectric Modulated TFET Based Biosensor.....	33
1.1.8	Literature Review of TFETs.....	34
1.1.8.1	Device Level Simulations Related Work.....	35
1.1.8.2	Previous Works Using TFETs in Circuit Design.....	41
1.1.8.3	Previous Work on TFET-Based Biosensors.....	43
1.2	Scope of the Thesis.....	44
1.2.1	Organization and Outline of the Thesis.....	45

CHAPTER 2

Performance Investigation of SiO₂/HfO₂ Stacked Gate Oxide Ge/Si Heterojunction TFET on SELBOX Substrate (STFET)

2.1	Introduction.....	49
2.2	TCAD Simulation Framework.....	51
2.2.1	2-D Schematic Structures of the Proposed TFETs.....	51
2.2.2	Possible Fabrication Steps.....	53
2.3	TCAD Simulation Methodology and Description of Models.....	54
2.3.1	Calibration of the Models.....	55
2.4	Results and Discussion.....	56
2.4.1	DC Performance Analysis.....	56
2.4.2	RF/Analog Performance Analysis.....	62
2.4.3	Temperature Impact Analysis.....	66
	Conclusions.....	70

CHAPTER 3

Impact of Interface Trap Charges (ITCs) on the Performance of SiO₂/HfO₂ Stacked Gate Oxide Ge/Si Heterojunction STFET

3.1	Introduction.....	71
3.2	Device Under Study.....	73

3.2.1	Schematic Structures.....	73
3.2.2	Fabrication Feasibility	73
3.2.3	Calibration of the Models	76
3.3	Results and Discussion.....	77
3.3.1	DC Performance Analysis.....	77
3.3.2	RF/Analog Performance Analysis	81
3.3.3	Linearity Performance Analysis	84
3.4	Conclusions	87

CHAPTER 4

Performance Investigation of Back Gated SiO₂/HfO₂ Stacked Gate Oxide Ge/Si Heterojunction STFET

4.1	Introduction	89
4.2	Device Under Study	90
4.2.1	Schematic Structure of Device.....	90
4.2.2	Possible Fabrication Steps	91
4.2.3	Simulation Setup and Models Approval.....	93
4.3	Results and Discussion.....	93
4.3.1	DC Performance Analysis.....	94
4.3.2	RF/Analog Performance Analysis	96
4.3.3	Linearity Performance Analysis	98
4.4	Design of BG-HJ-STFET based Inverter	102
4.5	Conclusions	104

CHAPTER 5

Performance Investigation of Back Gated SiO₂/Ferroelectric Stacked Gate Oxide Ge/Si Heterojunction STFET

5.1	Introduction.....	107
5.2	Device Under Study	108
5.2.1	Schematic Structure of the Device	108
5.2.2	Fabrication Process Flows	108

5.2.3	Models validation	111
5.3	Results and Discussion	111
5.3.1	DC Analysis.....	111
5.3.2	RF/Analog Analysis	115
5.3.3	Nonlinearity Distortion Analysis.....	116
5.4	Conclusion.....	120

CHAPTER 6

Performance Assessment of Back Gated Ferroelectric STFET as a Dielectric Modulated label-Free Biosensor

6.1	Introduction	121
6.2	Device Under Study	123
6.2.1	Device structure	123
6.2.2	Fabrication Feasibility	123
6.2.3	Calibration of the models.....	126
6.3	Results and Discussion.....	127
6.3.1	Impact of Charged Biomolecules.....	130
6.4	Conclusions	136

CHAPTER 7

Sensitivity Analysis of GaSb/GaAs Type-II Heterojunction STFET as a Dielectric Modulated Label-Free Biosensor

7.1	Introduction.....	137
7.2	Device for Study	139
7.2.1	Device Structure	139
7.2.2	Fabrication Process Flows and models validation.....	140
7.3	Results and Discussion	143
7.3.1	Analytical Modeling of Surface Potential	143
7.3.2	Electrostatic Analysis Using Neutral Charge Biomolecules	147

7.3.3	Impact of Negatively Charged Biomolecules.....	150
7.3.4	Impact of Positively Charged Biomolecules	152
7.3.5	Effect of drain and back gate biasing	153
7.3.6	Linearity Fit Verification.....	154
7.3.7	Comparison With the Biosensor Based TFET	155
7.4	Conclusions.....	156

CHAPTER 8

Summary Conclusion and Future Scope

8.1	Introduction.....	157
8.2	Chapterwise Contributions and conclusion	157
8.3	Future Scope of Work.....	161

References 163-188

Authors's Relevant Publicatins 189-190

LIST OF FIGURES

Figure 1.1	Microprocessor trends based on 42 years of experimental data [3].	04
Figure 1.2	The trend of supply voltage and threshold voltage scaling vs. technology generation. V_{DD} decreases with device dimensions, but V_T does not. From [2].	04
Figure 1.3	Trends of dynamic and static CMOS power, showing that static power [11].	07
Figure 1.4	Total power dissipation as a function of technology node, including an illustration of how the static power dissipation increases when technology advances to 65nm and beyond due to the large increase in the off-state current [12] [13].	08
Figure 1.5	Taxonomy of options for emerging logic devices as mentioned in ITRS 2.0 2015 edition [27].	10
Figure 1.6	Schematic of a Carbon Nanotube Field Effect Transistor (CNTFET) [28].	11
Figure 1.7	Schematic of a Carbon Nanotube Field Effect Transistor (CNTFET) [30].	11
Figure 1.8	Schematic of a nanowire field-effect transistor (CNTFET) [35].	12
Figure 1.9	Schematic of a negative gate capacitance field effect transistor (NGC-TFET) [37].	13
Figure 1.10	Plots of classical and quantum charge carrier transmission mechanism [43].	14
Figure 1.11	Schematic structure of conventional TFET [38].	15
Figure 1.12	Energy band diagram of conventional TFET in ON and OFF-state [38].	15

Figure 1.13	Shows the tunnel barrier as a triangular-shaped potential barrier [44].	16
Figure 1.14	Mention of tunnel FET in process, integration, and devices section of ITRS Report, 2013 [63].	20
Figure 1.15	A chronological division of the literature survey taken under this chapter.	21
Figure 1.16	Schematic structure of conventional TFET with SiO ₂ /High-k gate stacked engineering.	22
Figure 1.17	The Ferro dielectric TFET circuit diagram, which includes the TFET's C _{FE} , C _{SiO2} , and C _S [69].	24
Figure 1.18	Log scaled drain current plots for different CMOS devices such as MOSFET, TFET, and Fe-TFET [69].	25
Figure 1.19	Schematic structures of (a) bulk NMOS, (b) FD-SOIMOSFET and (c) SELBOX MOSFET [74], [75].	27
Figure 1.20	(a) Type-I or straddling gap heterojunction, (b) Type-II or staggered gap heterojunction, and (c) Type-III or broken-gap heterojunction [81].	28
Figure 1.21	Verilog-A model schematic.	29
Figure 1.22	Classification of biosensors based on the transducer [90].	32
Figure 1.23	2D schematic structure of TFET-based biosensor.	33
Figure 1.24	(a) Energy band diagram in OFF state (b) Energy band diagram in ON state.	33
Figure 1.25	Schematic view of the dielectrically modulated TFET [100].	34
Figure 1.26	Comparison of 65 nm state-of-art CMOS technology TFETs with MOSFETs, taken from [121].	38

Figure 2.1	2D cross-section view of (a) GSHJ-FD-SOITFET, and (b) GSHJ-STFET.	51
Figure 2.2	Possible fabrication steps for the proposed structure GSHJ-STFET [109].	53
Figure 2.3	Calibration of used model using SILVACO ATLAS TM TCAD tool: comparison of simulation data with experimental result of a SOI TFET (a) linear-linear scale, (b) log-linear scale [158], (c) Simulated and measured output characteristics. Symbols indicate measured data and solid lines the corresponding simulation.	56
Figure 2.4	Plots of gate leakage current for (a) without gate stacked i.e., SiO ₂ as the gate oxide, and (b) with gate stacked i.e., SiO ₂ /HfO ₂ as gate oxide of the HJ-STFET at $t_{EOT} = 1.312$ nm.	58
Figure 2.5	Plots of (a) I-V characteristics of both the presented TFETs and (b) energy band diagram for on and off state of the GSHJ-STFET.	58
Figure 2.6	Plots of (a) drain current for different values of SELBOX gap length and (b) drain current with the different positions of SELBOX gap of GSHJ-STFET.	59
Figure 2.7	Contour plots of non-local BTB e- tunneling rate of (a) GSHJ-FD-SOITFET, (b) GSHJ-STFET at $V_{DS} = 0.5$ V.	60
Figure 2.8	Plots of absolute electric field of proposed TFETs structures for SELBOX gap length at $V_{DS} = 0.5$.	60
Figure 2.9	Plots of surface potential of proposed TFETs structures for SELBOX gap length at $V_{DS} = 0.5$ V.	61
Figure 2.10	(a) Drain current versus and (b) output transconductance plots of both GSHJ-FD-SOITFET, and GSHJ-STFET at $V_{DS} = 0.5$ V.	61
Figure 2.11	Transconductance plots of both GSHJ-FD-SOITFET, and GSHJ-STFET at $V_{DS} = 0.5$ V.	63
Figure 2.12	Plots of C_{gg} , C_{gd} and C_{gs} for SELBOX gap length of the proposed TFET.	64

Figure 2.13	Plots of cut-off frequency SELBOX gap length of the proposed TFET.	65
Figure 2.14	(a) Cut-off frequency and (b) GWB plot of both GSHJ-FD-SOITFET, and GSHJ-STFET at $V_{DS} = 0.5V$.	65
Figure 2.15	(a) Transit time plots and, (b) TGF plots of both GSHJ-FD-SOITFET, and GSHJ-STFET at $V_{DS} = 0.5V$.	66
Figure 2.16	(a) TFP plots and, (b) maximum oscillation frequency plots of both GSHJ-FD-SOITFET, and GSHJ-STFET.	66
Figure 2.17	Variation of tunneling bandgap vs. temperatures at a drain voltage of 0.5 V.	68
Figure 2.18	Drain current plots at different temperatures of (a) GSHJ-FD-SOITFET, and (b) GSHJ-STFET.	69
Figure 2.19	Plots of (a) I_{ON}/I_{OFF} ratio vs. temperature and, (b) threshold voltage vs. temperature of GSHJ-FD-SOITFET, and GSHJ-STFET.	69
Figure 2.20	Subthreshold swing (SS) plots of GSHJSTFET and GSHJ-FD-SOITFET at various temperatures.	69
Figure 3.1	Schematic structures of (a) LGS-HJ-STFET, and (b) VGS-HJ-STFET.	74
Figure 3.2	Possible fabrication process steps of the proposed VGS-HJ-STFET [109].	74
Figure 3.3	Calibration of simulated result with the experimental result [159].	76
Figure 3.4	Plots of energy band diagram in (a) OFF and ON-state of LGS-HJ-STFET and (b) OFF and ON-state of VGS-HJ-STFET.	78
Figure 3.5	Plots of the electric field vs. device length of LGS-HJ-STFET and VGS-HJ-STFET at $V_{DS} = 0.5 V$.	79
Figure 3.6	Plots of (a) drain current, (b) transconductance, (c) output conductance, and (d) transconductance generation factor (TGF) with	81

respect to V_{GS} of LGS-HJ-STFET and VGS-HJ-STFET at $V_{DS} = 0.5$ V.

Figure 3.7	Variation of (a) SS for (-) ve ITC concentration, (b) SS for (-) ve ITC concentration, (c) V_{th} for (-) ve ITC concentration and (d) V_{th} for (+) ve ITC concentration of LGS-HJ-STFET and VGS-HJ-STFET, respectively.	82
Figure 3.8	Variation of (a) C_{gd} , (b) cut-off frequency (f_T), (c) transit time (t), and (d) gain-bandwidth product (GBP) for various trap concentration of LGS-HJ-STFET and VGS-HJ-STFET respectively.	83
Figure 3.9	Plots of (a) gm_3 and (b) zero crossover point (ZCP) of both TFETs at $V_{DS} = 0.5V$.	86
Figure 3.10	Comparative Plots of (a) VIP3, (b) IIP3 (c) IMD3, and (d) 1-dB compression point vs. V_{GS} of both TFETs.	87
Figure 4.1	2-D schematic structures of (a) SG-HJ-STFET, and (b) BG-HJ-STFET.	90
Figure 4.2	Fabrication Steps of BG-HJ-STFET.	91
Figure 4.3	Calibration of the ATLAS TCAD models: comparison of simulation data with the experimental result as reported [190].	93
Figure 4.4	Comparative plots of logarithmic drain current versus gate voltage of BG-HJ-STFET, (BG-STFET) and SG-HJ-STFET (SG-STFET) with the analysis of (a) Static Subthreshold swing (SS) and (b) Average subthreshold swing (SS).	95
Figure 4.5	Comparative plots of (a) surface potential, and (b) electric field at on-state for all the presented TFETs.	95
Figure 4.6	Comparative plots of (a) OFF-state energy band diagram, and (b) ON-state energy band diagram for all the presented TFETs.	96
Figure 4.7	Comparative plots of (a) transconductance (gm), and (b) intrinsic gate to drain capacitance (C_{gd}), for all the presented TFETs.	97

Figure 4.8	Comparative plots of (a) cut-off frequency (f_T), and (d) transit time (τ) for all the presented TFETs.	97
Figure 4.9	Comparative plots of (a) g_{m2} and (b) g_{m3} versus gate voltage at $V_{DS} = 0.5$ V.	100
Figure 4.10	Comparative plot of (a) zero crossover point and (b) 1-dB compression point of all the TFETs presented for study.	101
Figure 4.11	Plots of (a) VIP2, and (b) VIP3 of all mentioned devices with V_{GS} at $V_{DS} = 0.5$ V.	101
Figure 4.12	Plots of (a) IIP3 and (d) IMD3 of all mentioned devices with V_{GS} at $V_{DS} = 0.5$ V.	101
Figure 4.13	(a) Circuit diagram of inverter-based on BG-HJ-STFET (b) drain current versus V_{GS} plots of n-type and p-type BG-HJ-STFETs, (c) voltage transfer characteristics (VTC) of BG-HJ-STFET inverter (d) transient analysis of BG-HJ-STFET.	104
Figure 5.1	2D Schematic structure of BG-Fe-HJ-STFET.	108
Figure 5.2	Fabrication Steps of BG-Fe-HJ-STFET.	110
Figure 5.3	Calibrated transfer characteristics of the BG-Fe-HJ-STFET with the experimental data [159].	111
Figure 5.4	Energy band diagrams of (a) BG-Fe-HJ-STFET, (b) BG-HJ-STFET with respect to the device length in on and off-state and (c) The circuit diagram of ferroelectric oxide Fe-TFET including the C_{FE} , C_{SiO_2} and C_S for the TFET.	113
Figure 5.5	Plots of (a) $I_{DS}-V_{GS}$ of BG-Fe-HJ-STFET and BG-HJ-STFET, and (b) $I_{DS}-V_{DS}$ of the proposed TFET.	114
Figure 5.6	Plots of (a) Electric Field and (b) transconductance (inset I_D-V_{GS} graph of the proposed device at different gate material work function values, Ψ_s) of BG-Fe-HJ-STFET and BG-HJ-STFET w.r.t V_{GS} at $V_{DS} = 0.5$ V.	114

Figure 5.7	Plots of (a) C_{gd} , C_{gs} and C_{gg} , (b) cut-off frequency, f_T , (c) transit time, τ and (d) GBP of BG-Fe-HJ-STFET and BG-HJ-STFET vs. V_{GS} at $V_{DS} = 0.5$ V.	116
Figure 5.8	Variations of (a) gm_3 and (b) zero crossover point at $V_{DS}=0.5V$ of both studied TFETs.	118
Figure 5.9	Variations of (a) VIP2, (b) VIP3, (c) IIP3, and (d) IMD3 with V_{GS} at $V_{DS}=0.5V$ of both TFETs.	118
Figure 5.10	Plots of 1-dB compression point at $V_{DS}=0.5V$ of both TFETs.	119
Figure 6.1	2-D cross-section diagram of BG-Fe-HJ-STFET based Biosensor.	124
Figure 6.2	Possible fabrication process steps of the proposed BG-Fe-HJ-STFET [177].	126
Figure 6.3	Calibration graph of the proposed structure (BG-Fe-HJ-STFET) with prefabricated SOI TFET at $V_{DS} = 0.5V$, and $V_{DS} = 1.0V$ [158].	127
Figure 6.4	Plots of (a) ON-state energy band diagram, and (b) 2-D Electric field of BG-Fe-HJ-STFET based biosensor at $V_{GS} = 1V$, $V_{DS} = 0.5V$ and $t_c = 8$ nm.	128
Figure 6.5	Plots of (a) surface potential and (b) transconductance of neutral charge biomolecules of the proposed biosensor for the different biomolecules at $V_{DS} = 0.5$ V.	129
Figure 6.6	Plots of (a) cut-off frequency and (b) transit time of neutral charge biomolecules of the proposed biosensor for the different biomolecules at $V_{DS} = 0.5$ V.	130
Figure 6.7	Plots of transfer characteristics (a) neutral charge biomolecules (b) charged biomolecules (DNA) of HBG-STFET based biosensor at $V_{DS} = 0.5V$ and $t_c = 8nm$.	131
Figure 6.8	Plots of $I_{DS}-V_{GS}$ Sensitivity (a) neutral charge biomolecules (b) charged biomolecules (DNA) of BG-Fe-HJ-STFET based biosensor at $V_{DS} = 0.5V$ and $t_c = 8nm$.	131

Figure 6.9	I_{ON}/I_{OFF} ratio sensitivity plot of (a) neutral charge biomolecules (b) charged biomolecules (DNA).	132
Figure 6.10	(a) Threshold voltage (V_{th}) sensitivity plot of (a) neutral charge biomolecules (b) charged biomolecules (DNA).	134
Figure 6.11	Subthreshold swing (SS) sensitivity plot of (a) neutral charge biomolecules (b) charged biomolecules (DNA) of BG-Fe-HJ-STFET based biosensor at $V_{DS} = 0.5V$ and $t_c = 8nm$.	135
Figure 7.1	3D schematic structures of DC-HJ-STFET based biosensors.	139
Figure 7.2	Fabrication Steps of DC-HJ-STFET biosensor.	141
Figure 7.3	Calibration of the ATLAS TCAD tool by comparing the simulated drain current with experimental data of an SOI TFET reported in [158].	143
Figure 7.4	2D structure of DC-HJ-STFET based biosensors.	144
Figure 7.5	The surface potential plots along the length of the device at $V_{DS} = 1.0 V$, $V_{GS} = 1.0 V$ for different dielectric constant of the biomolecules.	147
Figure 7.6	Plots of (a) OFF-state and (b) ON-state energy band diagram of DC-HJ-STFET based biosensor for $k = 3, 7 \& 12$ at $t_c = 4nm$.	148
Figure 7.7	Plots of (a) 2-D Electric field and (b) drain current of DC-HJ-STFET based biosensor for $k = 3, k = 7 \& 12$ at $t_c = 4nm$.	148
Figure 7.8	2-D non-local band to band tunnelling (BTBT) contour DC-HJ-STFET based biosensor for (a) $k = 3$, (b) $k = 7$, & (c) $k = 12$ at $V_{GS} = 1V$, $V_{DS} = 1V$ and $t_c = 4 nm$.	149
Figure 7.9	Plots of (a) I_{ON} and I_{ON}/I_{OFF} sensitivity and (b) threshold voltage (V_T) and threshold voltage sensitivity (S_{VT}) of DC-HJ-STFET based biosensor for different dielectric constant of biomolecules for different value of cavity thickness at $V_{GS} = 1V$, $V_{DS} = 1V$.	150
Figure 7.10	Plots of (a) I_{ON} and I_{ON}/I_{OFF} sensitivity and (b) Threshold voltage and threshold voltage sensitivity (S_{VT}) of DC-HJ-STFET based biosensor	151

for different negative charged dielectric of biomolecules at $V_{GS} = 1V$, $V_{DS} = 1$.

- Figure 7.11** Plots of (a) I_{ON} and I_{ON}/I_{OFF} sensitivity and (b) threshold voltage and threshold voltage sensitivity of DC-HJ-STFET based biosensor for different dielectric constant of biomolecules at $V_{GS} = 1V$, $V_{DS} = 1V$. **151**
- Figure 7.12** Plots of (a) I_{ON} and I_{ON}/I_{OFF} sensitivity and (b) threshold voltage and threshold voltage sensitivity of DC-HJ-STFET based biosensor for different positive charged dielectric of biomolecules at $V_{GS} = 1V$, $V_{DS} = 1V$. **152**
- Figure 7.13** Plots of (a) I_{ON} and I_{ON}/I_{OFF} sensitivity and (b) threshold voltage (V_T) and threshold voltage sensitivity (S_{VT}) of DC-HJ-STFET based biosensor for different values of dielectric constant of biomolecules at $V_{GS} = 1V$, $V_{DS} = 1V$. **153**
- Figure 7.14** Plots of (a) drain current of DC-HJ-STFET based biosensor for different drain biasing (V_{DS}), and (b) I_D - V_{GS} characteristics of DC-HJ-STFET based biosensor for different V_{BG} (-3V to 3V). **153**
- Figure 7.15** Plots of (a) Linearity fit of I_{ON}/I_{OFF} sensitivity vs. dielectric constant for (+)ve charged density biomolecules, and (b) Comparison of I_{ON}/I_{OFF} sensitivity of DC-HJ-STFET based biosensor with other TFETs **155**

LIST OF TABLES

Table. 1.1:	Scaling of the device dimensions and circuit parameters [10].	06
Table. 1.2:	Modes of operation in TFET, convention of source and drain regions, and biasing condition [38].	14
Table. 2.1:	Studied devices parameters.	52
Table. 2.2:	Values of DC parameters of the studied TFETs structures.	62
Table. 2.3:	Comparison of RF/analog parameters of all given structures.	67
Table. 3.1:	Device specifications.	75
Table. 3.2:	Comparative table of dc parameters between LGS-HJ-STFET and VGS-HJ-STFET for negative, positive, and neutral interface trap charges (ITCs) with $\pm 1 \times 10^{12}/\text{cm}^2$ concentration.	80
Table. 3.3:	Comparative table of analog/RF parameters between LGS-HJ-STFET and VGS-HJ-STFET for negative, positive, and neutral interface trap charges (ITCs) with $\pm 1 \times 10^{12}/\text{cm}^2$ concentration value.	84
Table. 4.1:	Device Parameters for the simulation.	92
Table. 4.2:	Performance comparative table among all the studied	96

TFETs.

Table. 5.1:	List of device dimensions and structural parameters.	109
Table. 5.2:	Comparison of the results of the mentioned TFET structures with the published article [76, 212].	119
Table. 6.1:	Device Specifications	125
Table. 6.2:	Comparison of the sensitivity with the ref. [220], [250].	136
Table. 7.1:	GaSb and GaAs Materials Parameters for the Simulation study [222], [245].	140
Table. 7.2:	Some important biomolecules with dielectric Constant value [222] [226], [228], [237]-[238].	140
Table. 7.3:	List of devices (DC-HJ-STFET) dimensions and structural parameters.	142
Table. 7.4:	Proposed TFET Sensor (DC-HJ-STFET) Sensitivity for Neutral, (+)ve Charged and (-)ve Charged Biomolecules.	154
Table. 7.5:	I_{ON} and sensitivity comparison of DC-HJ-STFET biosensor with other reported TFET biosensors.	156

LIST OF ABBREVIATIONS

Abbreviation	Details
BTBT	Band-to-band Tunneling
TFET	Tunnel Field Effect Transistor
2-D	Two Dimensional
3-D	Three Dimensional
SCEs	Short Channel Effects
DG	Double Gate
BG	Back Gate
MOS	Metal Oxide Semiconductor
FET	Field Effect Transistor
MOSFET	Metal Oxide Semiconductor Field Effect Transistor
SOI	Silicon-on-Insulator
IC	Integrated Circuit
SS	Subthreshold Swing
SMG	Single Material Gate
TMG	Triple Material Gate
DMG	Dual/Double Material Gate
CMOS	Complementary Metal Oxide Semiconductor
BJT	Bipolar Junction Transistor
TEM	Tunneling Electron Microscope
BOX	Buried Oxide
SELBOX	Selective Buried Oxide
TCAD	Technology Computer-Aided Design

ITRS	International Technology Roadmap for Semiconductors
EOT	Equivalent Oxide Thickness
NW	Nanowire
ALD	Atomic Layer Deposition
L-BTBT	Lateral-Band to Band Tunneling
DM	Dual Material
JLFET	Junctionless Field Effect Transistor
SRAM	Static Random-Access Memory
TFP	Transconductance Frequency Product

LIST OF SYMBOLS

Symbol	Details
f_T	Unity Gain Frequency
f_{max}	Maximum Frequency of Oscillation
E_g	Energy Band Gap
Vel_0	Ballistic Velocity
E_C	Conduction Band energy
E_V	Valance Band Energy
q	Electronic Charge
T	Temperature in Kelvin
KT	Thermal Energy
V_T	Thermal Voltage
V_{th}	Threshold Voltage
I_D	Drain Current
$N_{S/D}$	Source/Drain Doping
N_{ch}	Channel Doping
g_m	Transconductance
g_d	Output-Conductance
I_{ON}	ON Current
I_{OFF}	OFF Current
I_{leak}	Leakage Current
V_{GS}	Gate-to-Source Voltage
V_{DS}	Drain-to-Source Voltage
t_{si}	Channel Thickness
w_{si}	Width of the Channel
t_{ox}	Oxide Thickness

LIST OF SYMBOLS

R	Radius of the Channel
L	Length of the Channel
ψ	Potential Function
nm	Nanometer
V	Voltage
L	Channel Length
eV	Electron Volt
mA	Milli Ampere
μm	Micro Meter
V_f	Quasi-fermi Level
n_i	Intrinsic Concentration
m_e	Effective Mass
h	Plank Constant
λ	Wave Function
U	Potential Energy
E	Discretized Energy
r	Radial Coordinate
z	z-Coordinate
θ	Radial Coordinate
μ	Mobility
V_{tL}	Long Channel Threshold Voltage
SS	Subthreshold Slope

Abstract

The semiconductor industry has been on the lookout for alternative to MOSFETs due to the inability of MOSFETs to remain immune to downscaling in the term of performance. The ultimate objective at present is to design devices with principle of operation different from MOSFETs. Researchers have proposed novel devices which possess promising prospects as compared to MOSFETs in terms of performance from the perspective of present requirements of the semiconductor industry. This thesis presents work on one such emerging device, the Tunnel Field Effect Transistor (TFET). The device geometry of TFET is similar to MOSFET except that its source and drain regions are oppositely doped with an intrinsic channel. The device operates by interband (Zener) tunneling caused by electric field modulation at source/channel junction by a controlling electrode. In this thesis work till chapter 5, I have done the performance investigation of some heterojunction TFETs on SELBOX substrate with and without back gated. All chapters contain extensive electrostatic analysis such as DC, RF/analog, and linearity parameters. In chapter 6 and chapter 7, I have studied the dielectric modulation-based label-free biosensor of the proposed structure and compared it to state-of-art sensors. The works presented in the different chapters are summarized below.

Chapter 1 this chapter introduces the thesis by briefly presenting the drawbacks of the MOSFET including the effects of scaling, and the emergence of novel semiconductor devices. Various emerging device structures have been introduced to sustain MOSFET scaling for future generation IC technology. It has been discussed that tunnel field-effect transistors (TFETs) have a huge potential for reducing short channel effects (SCEs) that occur when MOS devices have been scaled. It comments on the working principle of TFETs and their suitability for low-power electronics applications. The general review of some important state-of-the-art literatures related to TFETs shows that there are ample opportunities for theoretical investigation of the electrical performance of TFET on SELBOX substrate with gate oxide engineering as well as low bandgap engineering. Circuit level-based study was also reviewed in order to make a better understanding of the TFETs in circuit-level applications. In the addition, Furthermore, we conducted a literature review on dielectric modulated biosensors based on the TFET technology.

Based on the literature survey, the scopes of the present thesis have been outlined in the last section of this chapter.

Chapter 2 this chapter proposes an electrostatic comparison between conventional fully depleted SOI TFET and proposed Heterojunction TFET on SELBOX Substrate. This chapter discusses the advantages of the proposed TFET structure over the conventional fully depleted SOI TFET structure. The major observations can be given as follows:

- This work investigates the DC and Analog/RF performance of a newly suggested GSHJ-STFET-based TFET structure with stacked $\text{HfO}_2/\text{SiO}_2$ gate and Ge (source)/Si (channel) heterojunction.
- The rapid rate of BTB tunneling of carriers from the source to the channel region is due to the presence of germanium (a low bandgap material) in the source region.
- It has been shown that the SELBOX structure demonstrates the advantages over SOI and bulk structures. So, it can be considered a good option while selecting between SOI and bulk structures. This is mainly due to the gap present in the buried oxide in the SELBOX structure.
- The SELBOX substrate has been used in the proposed TFET to reduce the lattice heat and improve the I_{ON}/I_{OFF} ratio.
- Vertical gate stacked $\text{SiO}_2/\text{HfO}_2$ is highly responsible for the reduction of the gate leakage current due to the higher physical thickness of the gate oxide layer. The proposed TFET structure with SELBOX improves both DC and RF characteristics.

Chapter 3 In this chapter, we have investigated the influence of both the donor and acceptor type interface trap charges (ITCs) on the reliability of LS-STFET and VS-STFET in terms of their DC, analog/RF, and linearity parameters. This is a comparative analysis work based on their DC/RF and linearity parameters. The major observations in chapter 3 are given following.

- The presence of ITCs causes more severe effects on the performance degradation of VS-STFET than the LS-STFET structure. Thus, the proposed LS-STFET is more reliable than the VS-STFET device structure.

- Therefore, the LS-STFET device structure can be considered a promising MOS device for low-power and high-frequency applications.

Chapter 4 this chapter reports the design and device-level simulation analysis of a back-gated Ge/Si heterojunction TFET on SELBOX substrate (BG-HJ-STFET). There are some major points listed below about chapter 4:

- The proposed structure implements a stacked gate oxide where the conventional SiO₂ is replaced by a SiO₂/HfO₂ in a stacked manner to increase its On-current.
- A back gate (BG) is also considered in the proposed TFET to enhance the device-level performance.
- Investigation of DC, RF, and linearity parameters such as drain current, transconductance, electric field, parasitic capacitance, cut-off frequency (f_T), gain-bandwidth product (GBP), intrinsic delay (τ), higher-order of g_m (g_{m2} , g_{m3}), VIP2, VIP3, IIP3, IMD3, and 1-dB compression point are carried out for the proposed TFET and the results are compared with other conventional structures.
- Finally, we have discussed back gate effects on the performance of the proposed TFET.
- Performance evaluation shows that BG-HJ-STFET is a suitable candidate for distortionless and high-frequency applications.

Chapter 5 this chapter reports the device-level performance of a back gated ferroelectric heterojunction TFET on SELBOX substrate (BG-Fe-HJ-STFET). The proposed structure implements a stacked gate oxide where the conventional SiO₂ is replaced by a SiO₂/ferroelectric oxide in a stacked manner to increase its on-current. The following major points of this chapter are listed below.

Investigation of DC, RF, and linearity parameters such as drain current, transconductance, electric field, parasitic capacitance, cut-off frequency (f_T), gain-bandwidth product (GBP), intrinsic delay (τ), higher-order of g_m (g_{m2} , and g_{m3}), VIP2, VIP3, IIP3, IMD3, and 1-dB compression point are carried out for the proposed TFET and the results are compared with other conventional structures.

